International Journal of Nanomedicine

Dovepress
Taylor & Francis Group

Open Access Full Text Article

ORIGINAL RESEARCH

Nanoformulations Downregulating METTL16 Combined with mRNA Tumor Vaccines Suppress Triple-Negative Breast Cancer and Prevent Metastasis

Runying Wang[1,*], Yufeng Zhang[1,*], Shubo Du[1], Yanhua Li[2], Yanying Ren[3], Jiaqi Lin[1]

[1]MOE Key Laboratory of Bio-Intelligent Manufacturing, School of Bioengineering, Dalian University of Technology, Dalian, Liaoning, 116024, People's Republic of China; [2]Department of International Medical Department, the Second Affiliated Hospital of Dalian Medical University, Dalian, Liaoning, 116021, People's Republic of China; [3]Hernia and Colorectal Surgery Department, the Second Affiliated Hospital of Dalian Medical University, Dalian, Liaoning, 116023, People's Republic of China

*These authors contributed equally to this work

Correspondence: Jiaqi Lin, School of Bioengineering, Dalian University of Technology, Dalian, Liaoning, People's Republic of China, 116024, Tel +86 13125472686, Email jqlin@dlut.edu.cn; Yanying Ren, Hernia and Colorectal Surgery Department, the Second Affiliated Hospital of Dalian Medical University, Dalian, Liaoning, People's Republic of China, 116023, Email renyanying@dmu.edu.cn

Purpose: Triple-negative breast cancer (TNBC) poses a significant threat to women's health due to its high malignancy and recurrence. Traditional treatments such as surgical resection, radiotherapy, and chemotherapy are no longer sufficient to meet clinical needs. Based on prior research that identified METTL16 as a potential target for TNBC, this study aimed to develop a nanoformulation to mitigate the malignancy of TNBC by silencing METTL16. The integration of this formulation with emerging mRNA tumor vaccines aimed to effectively inhibit the growth and metastasis of TNBC.

Research Methods: Using microfluidic technology, efficient siRNA encapsulation in lipid nanoparticle (LNP) yielded LNP/siMETTL16 and selective organ-targeting LNP/siMETTL16 (SORT-LNP/siMETTL16). Initially, the antitumor properties of LNP/siMETTL16 were evaluated at the cellular level. Subsequently, the antitumor properties were explored in mouse subcutaneous TNBC models with LNP/siMETTL16 (intratumoral injection) and mRNA tumor vaccines (intramuscular injection). The combined inhibition of TNBC lung metastasis by SORT-LNP/siMETTL16 (intravenous injection) and mRNA vaccine (intramuscular injection) was also investigated.

Results: Cellular experiments demonstrated the efficient silencing effect of LNP/siMETTL16, leading to inhibition of tumor cell activity. The combination of LNP/siMETTL16 and LNP/mMUC1 significantly suppressed subcutaneous tumor growth, achieving an inhibition rate of 66.0%. Furthermore, the combination of SORT-LNP/siMETTL16 and mRNA tumor vaccines markedly alleviated TNBC lung metastasis.

Conclusion: This study provides evident support for the application and translation of METTL16 as a therapeutic target and offers a novel strategy for TNBC combined treatment in clinical settings.

Keywords: triple-negative breast cancer, METTL16, gene silencing, mRNA tumor vaccine, combined therapy

Introduction

As we all know, breast cancer has become one of the most prevalent malignant tumors worldwide.[1] Although the traditional therapy for breast cancer has been able to achieve good therapeutic effect, clinical patients still face unsatisfactory prognoses, particularly those with advanced and metastatic triple-negative breast cancer (TNBC).[2,3] Consequently, developing new therapeutic targets and strategies has become a critical challenge in breast cancer treatment.[4,5]

Received: 5 February 2025
Accepted: 5 July 2025
Published: 11 July 2025

The mRNA-related vaccine can achieve immune mediated tumor destruction by inducing the immune response to tumor-specific antigen.[6,7] In addition, the mRNA vaccine has the advantages of flexible coding of antigen sequence, simple production, and short development cycles.[8] Currently, various mRNA tumor vaccines have shown encouraging results in cancer treatment.[9–12] At present, a variety of antigens have been used in the research of tumor vaccines, of which MUC1 has been widely used in clinic as a tumor vaccine.[13,14] Human mucin 1 (MUC1) is a transmembrane mucin glycoprotein and is usually overexpressed in most tumor cells,[15–17] which makes MUC1 one of the main targets for tumor-specific immunotherapy. At present, it has been proven that the immunosuppressive microenvironment in breast cancer can inhibit the tumor-specific immune response caused by the MUC1 vaccine.[18,19] This leads to monotherapies often failing to achieve complete tumor suppression, likely due to the multifaceted nature of cancer pathogenesis. Fortunately, recent studies have shown that combination of tumor vaccines with other treatment methods (for example: knock-down the gene of Mlh1, immune checkpoints, delivering immune factors/T cells) can promote vaccine efficacy by reducing the malignancy degree of tumors and increasing immune surveillance and modulating tumor microenvironment.[20–24] Thus, these suggest that combining immunotherapy with tumor vaccines may lead to efficient tumor suppression.

In previous research, our team has thoroughly demonstrated the regulatory mechanism of METTL16 (a methyltransferase-like protein) of breast cancer.[25] Knocking out the METTL16 gene in breast cancer can significantly inhibit their proliferation, migration, and invasion capabilities. Since METTL16 regulates the proliferation of TNBC through FBXO5, and FBXO5 is negatively correlated with endoplasmic reticulum (ER) stress,[26] and apoptosis induced by ER stress is closely correlated with immunogenic microenvironment,[27,28] this provides a new potential target for breast cancer treatment. Therefore, we hypothesize that developing gene-regulating nanomedicines targeting METTL16 using siRNA gene silencing technology, combined with mRNA tumor vaccines is expected to achieve efficient suppression of TNBC.

Given the easy degradation of nucleic acid drugs and their lack of efficient cellular internalization, they often need the protection of a carrier to better function.[29] Lipid-based carriers are widely used in the in vivo delivery of nucleic acids due to their good encapsulation properties and high delivery efficiency.[30] Therefore, this study mainly used lipid nanoparticle (LNP) to effectively encapsulate siRNA to obtain a new nanoformulation LNP/siMETTL16. First, silencing effect and inhibitory effect on tumor cell activity were verified at the cellular level. Furthermore, based on the 4T1 antigen target MUC1, the vaccine LNP/mMUC1 was successfully constructed.[31] Finally, the high efficiency of LNP/siMETTL16 and LNP/mMUC1 combined tumor inhibition was verified in the 4T1 tumor-bearing mouse model (Scheme 1).

In addition, research shows that LNPs usually accumulate in the liver and are internalized by hepatocytes after intravenous injection so that nanoparticles difficult to surpass the transport barrier caused by the liver to arrive target-specific organs.[32] Given the high lung metastasis rate of breast cancer in clinical practice, we introduced a lung targeting vector SORT-LNP (Selective Organ-Targeting LNP) to deliver siMETTL16 to lung lesions and proved its efficient inhibitory effect on 4T1 breast cancer lung metastasis in combination with vaccines. In short, this work successfully developed LNP/siMETTL16 based on LNP delivery technology and siRNA gene silencing technology. This preparation represents an application transformation of METTL16 therapeutic target discovered in the early stage. The combined therapy proposed based on LNP/siMETTL16 and mRNA tumor vaccines will surely provide a new therapeutic strategy for clinical breast cancer treatment.

Materials and Methods

Chemicals and Reagents

Cholesterol, DMG-PEG_{2000}, and DSPC were sourced from Sinopeg Biotech (Xiamen, China). The cationic lipid SM102 was acquired from Jenkem Technology (Beijing, China). DOTAP was purchased from MeloPEG Technology (Shenzhen, China). 1,1'-dioctadecyltetramethyl indotricarbocyanine iodide (DIR) was obtained from Absin Bioscience Inc (Shanghai, China). Luciferase mRNA was obtained from PROXYBIO (Dalian, China) and D-Luciferin was purchased from Yeasen (Shanghai, China). BCA protein concentration assay kit and Cell Counting Kit-8 were obtained from Beyotime Biotechnology (Shanghai, China). Red blood cell lysis buffer (420301) was obtained from Biolegend (USA). The METTL16 (ab313743, 1:1000) antibody was purchased from Abcam (USA). The anti-GAPDH (af7021, 1:3000) antibody was acquired from Affinity Biosciences (USA). Goat anti-Rabbit IgG (HRP Conjugate, BL052A, 1:2000) was sourced from Biosharp (Hefei, China). All antibodies used for flow cytometry included CD16/32 (E-AB-F0997A), F4/90 (E-AB-F0995H), CD45 (E-AB-F1136S),

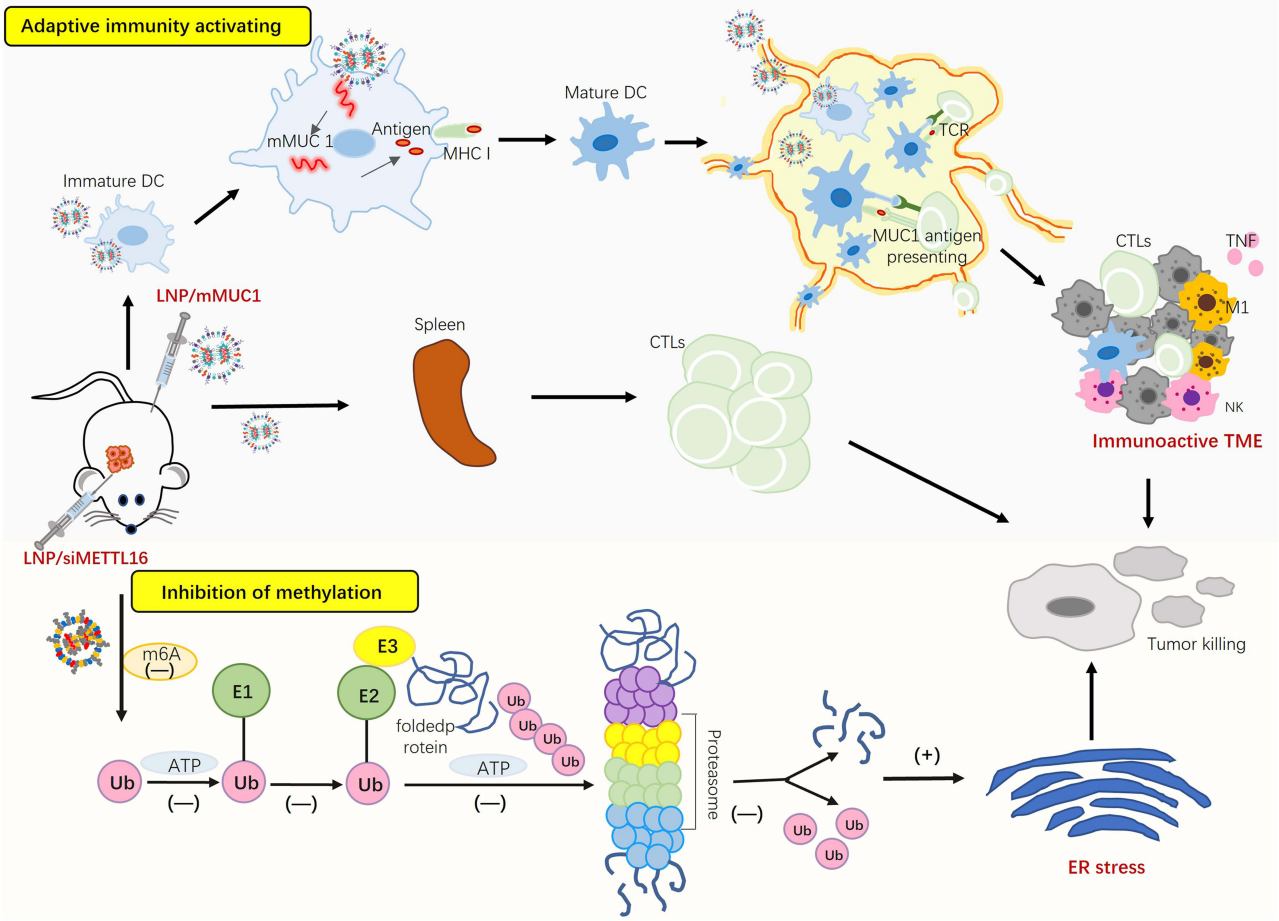

Scheme 1 A working model of combination mRNA vaccines of LNP/MUC1 and LNP/siMETTL16 for TNBC. In this working model, inhibiting the methylation of METTL16 could promote ER stress-induced cell apoptosis by decreasing the expression of FBXO5, thereby preventing the progression of tumor cell. Meanwhile, mRNA vaccine of LNP/MUC1 could stimulate the adaptive immune activating and induce the formation of immune microenvironment together that promoted the apoptosis of tumor cells, thereby induced cell apoptosis.

CD44 (E-AB-F1100UD), CD62L (E-AB-F1011E) were obtained from Elabscience (China); CD3 (100,306), CD8a (100708), CD80 (104,705), CD11c (117307) were obtained from Biolegend (USA).

Cell Lines and Animals

4T1 murine cells (triple-negative breast cancer) were provided by the Cell Bank of the Chinese Academy of Sciences (Shanghai, China). 4T1 cells were cultured in 1640 medium which supplemented with 10% fetal bovine serum (FBS), 1% antibiotics (penicillin and streptomycin), and incubated at 37 °C humidified environment with 5% CO_2 supply. Female BALB/C mice (5–6 weeks) was gained from Liaoning Changsheng biotechnology. 4–6 weeks BALB/C female mice were housed in the environment at 22±2°C and 50–60% humidity, with a 12h light-dark cycle. All animal experiments were conducted in accordance with the National Institute Guide for the Care and Use of Laboratory Animals and approved by the Biological and Medical Ethics Committee Dalian University of Technology (approval number: DUTSBE241231-01).

siMETTL16 and mMUC1 Sources

The design and production of siMETTL16 were entrusted to Haixing Biosciences (Suzhou, China), and the sequence information was presented in Table S1. The MUC1 antigens utilized wild-type full-length sequences, augmented with T7 promoter, 5' untranslated region (UTR), 3' UTR, and a poly (A) tail to form complete constructs. These sequences were custom-cloned and inserted into a plasmid as cloning vectors by GenScript Biotech Corporation (Nanjing, China), and PROXYBIO (Dalian, China) was entrusted with the synthesis of the final mRNA.

https://doi.org/10.2147/IJN.S520329

Preparation of LNP/siMETTL16 and LNP/mMUC1

LNP/siMETTL16 was synthesized through the integration of lipids and RNA within a microfluidic chip. Under acidic conditions, cationic lipids can bind to negatively charged mRNA by electrostatic interaction. The lipid solution dissolved in ethanol was mixed with the citric acid aqueous solution dissolved in mRNA and precipitated, that was, the lipid nanoparticles containing mRNA were self-assembled. In our experiment, a microfluidic mixing method was used to form LNP with uniform and controllable particle size between lipid solution and mRNA solution in a microfluidic mixer. The initial product of LNP contained high concentration of ethanol, and the residual ethanol needed to be removed by dialysis. Specifically, SM102, DSPC, cholesterol, and DMG-PEG_{2000} were dissolved and added respectively in ethanol at a precise molar ratio of 50:10:38.5:1.5. During SORT-LNP preparation, SM102, DSPC, cholesterol, DMG-PEG_{2000} and DOTAP were dissolved in ethanol at a precise molar ratio of 25:5: 19.3:0.8:50.[33] Meanwhile, siRNA was dissolved in a citrate buffer (pH=4) to constitute the aqueous phase, with a nitrogen-to-phosphate ratio of 3:1 on the ionizable lipids to siRNA. The ethanol mixture solvent and aqueous phases were combined using syringe pumps (LONGER) at a volume ratio of 3:1, then incubated for 10 min at room temperature. The mixture was dialyzed (MW=14kDa, Biosharp) against PBS at 4°C for more than 6h. The hydrodynamic diameter and polydispersity index of LNPs were meticulously measured at 25 °C by Litesizer™100 (Anton Paar). It was noticed that ensure the uniformity of the sample and mix the sample well before measurement. The synthesis procedures for LNP/mMUC1 mirrored those of LNP/siMETTL16 with a nitrogen-to-phosphate ratio of 6:1. The encapsulation efficiency was determined using Quant-iT RiboGreen RNA assay (Thermo Fisher Scientific). The principle was to determine the concentration of free RNA in LNP-RNA solution and the concentration of all RNA in the solution after the LNP structure was destroyed by Triton-100, and the difference between the two was the concentration of RNA trapped inside the LNP. Briefly, siRNA standard serial dilution series was prepared (2000–62.5ng/mL) and formulations were diluted to 500ng/mL. Samples were incubated with RiboGreen reagent (diluted 200× in PBS) and amount of unencapsulated siRNA was measured at 485/535nm (λEx/Em) on Infinite F/M200 Pro microplate reader (Tecan). LNP formulations were disrupted with 0.5% Triton X-100 to quantify the total amount of RNA (free and encapsulated). The %EE was then calculated as: $\%EE = (1-mRNA_{free}/mRNA_{total}) \times 100$. All the above instruments are adhered strictly accordance with the manufacturer's instructions.

Cytotoxicity Experiments

CCK8 was used to assess the impact of LNP/siMETTL16 on the viability of 4T1 cells. Initially, 4T1 cells with good growth state were digested, centrifuged and re-suspended to prepare single-cell suspension. After cell counting with a blood cell counting plate, the cell suspension was added to the 96-well plate with 2000 cells (100μL) per well, each group were performed in triplicate. Treated with various formulations (siRNA, 250ng/well) for a co-incubation period of 24 or 48 hours after overnight culture in 37°C incubator and wall attachment. Subsequently, we added a medium containing CCK8 (10%) to the well and incubated for 2 hours. Finally, the absorbance at 450nm (Infinite Plex, TECAN) was measured, and the cell viability was calculated accordingly.

Clone Formation Assay

A 12-well plate was applied to seed 4T1 cells from each treatment group (at a denseness of 500 cells) and cultivated overnight until they adhere to the wall. Subsequently, LNP/siMETTL16 (siRNA, 0.5μg/well) was added and incubated in a constant temperature incubator for 24 hours. Then poured out the culture medium and washed it with PBS. The cells were fixed with 4% paraformaldehyde for 15 minutes. Subsequently, 1% crystal purple (Sigma-Aldrich) was stained for 10 minutes. Then the cells were gently and slowly rinsed with running water. Finally, they were observed under an AX-70 fluorescence microscope (Leica Microsystems Inc., Germany).

Wound Healing Assay

For the migration assay, 4T1 cells in logarithmic growth phase were seeded into 6-well plates. When the cell density reached 80–90% confluence, scratch wounds were introduced and washed by washing buffer (PBS). Subsequently, different formulations were added to the wells and were added to the wells (siRNA, 1.5μg/well), and cells were further cultured in a 2% serum condition for 24 hours. Finally, we observed the scratches at the 0th and 24th hours and recorded the width of the scratches. Images were taken, and migration rate was analyzed using ImageJ software.

In vivo Fluorescence Imaging

We employed a fluorescence imaging system sourced from Tiannon (Shanghai) to assess the in vivo delivery efficacy of SORT-LNP. DIR dye was doped into the LNP lipid phase at a molar ratio of 1%. The preparation process of LNP/Luc-mRNA/DIR was the same as that of LNP/MUC1.

4–6 weeks BALB/C female mice (18–22g) were divided into four groups, with 3 mice in each group. They were i.v. injected separately with LNP/Luc-mRNA/DIR formulations (mRNA, 5μg, 0.25mg/kg, 6h); SORT-LNP/Luc-mRNA/DIR formulations (mRNA, 5μg, 0.25mg/kg, 6h). Animals were anesthetized under isoflurane, the DIR dye was evaluated by live animal bioluminescence imaging. At the same time, D-Luciferin (150mg/kg) was introduced by intraperitoneal injection. After anesthesia, the luciferase expression was evaluated. Afterward, these mice were killed, and different organs (heart, lung, liver, spleen, kidney) were collected for ex vivo imaging.

In vivo Anti-Tumor Experiment

4T1 cells with good growth state were digested, centrifuged and re-suspended to prepare single-cell suspension and counted, then store cells suspension at 4°C. 4T1 cells (1×10^5 cells) were injected subcutaneously on the dorsal region of per mice (Day −6). Then the mice harboring tumors were arbitrarily assigned to four groups, with 5 mice in each group. Divided into PBS group (G1), LNP/siMETTL16 group (G2), LNP/mMUC1 treatment group (G3), LNP/siMETTL16 and LNP/mMUC1 combination treatment group (G4). Administration of the LNP/mMUC1 vaccine (mRNA, 350μg/kg) commenced on days 0 and 6 via intramuscular injection. Meanwhile, LNP/siMETTL16 (siRNA, 100nmol/kg) was injected intratumorally on days 1, 4, 7, and 9. Commencing from day 0, the mice were monitored for changes in both body weight and tumor size every other day. Tumor volume was determined using the formula V = (Length×Width^2) / 2, where length and width signify the greatest and perpendicular shortest dimensions of the tumor, respectively. On day 14, all mice were euthanized, and tissues were taken for further examination. Construction methods of breast cancer metastatic tumor models: the 4T1 cells (2×10^6 cells) were i.v. injected into mice for 6 days (3 in each group). Then LNP/MUC1 (mRNA, 350μg/kg) was i.v. injected on days 0 and 5. Meanwhile, the SORT-LNP/siMETTL16 (siRNA, 200nmol/kg) formulation was i.v. injected on days 1, 4, 7. On the 10th day, all the experimental mice were euthanized, and the lung tissues were taken out for preservation at the same time. Subsequently, the slices were sectioned for H&E staining and observed. All experiments were supported by Dalian University of Technology.

Flow Cytometry Analysis

First, removed tumour tissues using a sterile blade and digested in digestion medium (1mg/mL collagenase I200ug/mL DNase I) for 30min. Next, filter the tissues solution and wash it with PBS. Then, perform centrifugation at 4°C (350g, 8 min) to obtain the cell precipitate. Subsequently, resuspend the cell precipitate in red blood cell lysis buffer and incubate on ice for 3 minutes. Finally, the cell solution washed with 1× PBS and centrifuged again at 350g for 8 min to obtain a cell pellet. Next, 1×10^6 cells were suspended in 100μL of PBS and the single-cell suspensions were stained with anti-mouse CD16/32 on ice for a duration of 10 minutes to block nonspecific staining. Then, the cells were stained on ice for 30 min using the following combinations: CD45/CD3/CD8 (Tumor); CD45/CD80/CD11c/F4/80 (Tumor); CD8/CD62L/CD44 (Spleen). Post incubation, analysis using a Cyto-FLEX flow cytometer (Beckman Coulter).

HE Staining

Fixed and encapsulated the tumor tissue. Subsequently, 6μm sections were taken and incubated in hematoxylin for 3 minutes, then eosin staining for 45 seconds. Finally, dehydration was carried out and imaging was performed under an AX-70 fluorescence microscope (Servicebio, Wuhan).

Statistical Analysis and Schematic Diagram

Data were presented as the mean ± standard deviation. GraphPad Prism 9.5 software was used for analyzing statistical significance. Significant differences were assessed using a *t*-test or one-way ANOVA (*$p < 0.05$, **$p < 0.01$, ***$p < 0.001$, ****$p < 0.0001$).

Results

Preparation and Characterization of LNP/siMETTL16

LNP, known for their efficient delivery and low toxicity, have been extensively used for in vivo nucleic acid delivery.[34] In this study, we employed microfluidic technology to encapsulate siMETTL16 into LNPs (Figure 1A), achieving an encapsulation efficiency of 95.2% (Table S2). It is well-established that the size of nanomedicine directly affects its circulation and distribution in vivo.[35] The hydrodynamic diameter of LNP/siMETTL16 was measured at about 131.86 nm, within the optimal range of 50–200 nm, conducive to cellular uptake and systemic circulation (Figure 1B). Meanwhile the hydrodynamic diameter (Figure S2A), PDI and the mRNA encapsulation efficiency of LNP/MUC1 were also determined (Table S2). Furthermore, Western blotting (WB) analysis confirmed that LNP/siMETTL16 effectively silenced METTL16 expression in 4T1 cells. Compared to the negative control (empty LNP), the protein expression in the treated group (LNP/siMETTL16) was reduced to 57%, demonstrating the gene-silencing capability of the nanoformulation (Figure 1C and D).

Inhibition of Breast Cancer Cells by LNP/siMETTL16

Following successful nanoformulation formulation, its antitumor effects on 4T1 cells were evaluated using wound healing assays, crystal violet staining, and CCK8 assays. As shown in Figure 1E and F, compared to the Blank group (PBS) and Negative group (empty LNP), the Treated group (LNP/siMETTL16) exhibited significant inhibition of tumor cell migration. Figure 1G shows that the crystal violet staining results after cells were co-incubated with nanomedicine for 24 hours. The purple area distribution in the Treated group was significantly lower than that in the control group, indicating that LNP/siMETTL16 also had an inhibitory effect on cell colony formation. Additionally, the cytotoxicity detected using the CCK8 assay showed similar results, with the nanoformulation inhibiting cell proliferation to some extent after 24 hours and 48 hours of co-incubation with cells (Figure 1H). These findings demonstrate that LNP/siMETTL16 has the potential to inhibit tumor growth and migration in vivo.

Combined Inhibition of 4T1 Breast Cancer by LNP/siMETTL16 and LNP/mMUC1

Given the inhibitory effect of LNP/siMETTL16 on tumor cells in vitro, we established a 4T1 tumor-bearing mouse model to investigate its antitumor efficacy in vivo and its combined effect on the therapeutic performance of the mRNA tumor vaccine. The treatment regimen was illustrated in Figure 2A and B. Beginning on day 0, therapeutic administration of LNP/mMUC1 was initiated through intramuscular injection, whereas treatment with LNP/siMETTL16 commenced via intratumoral injection from day 1 onward. Tumor size and body weight were monitored throughout, and the mice were euthanized on day 14 for further tissue analysis.

No significant weight loss was observed across treatment groups (Figure 2C), indicating the feasibility and safety of the therapeutic strategy. Compared with the PBS group (G1), the LNP/siMETTL16 group (G2) showed a significant delay in tumor growth rate, which indicated that the nanoformulation has a certain anti-tumor activity (Figure 2D and H). Similarly, the mRNA vaccine alone (G3) demonstrated antitumor efficacy, indicating the successful activation of tumor-targeted immune responses. However, monotherapy did not exhibit highly efficient antitumor effects, likely due to the complex pathogenic mechanisms of breast cancer that limit the efficacy of single treatments.[36,37] Fortunately, the combined treatment group (G4) achieved more favorable results, increasing the inhibition rate from 46.8% (G2) and 34.0% (G3) to 66.0% (Figure 2E–G). This result demonstrates the superiority of combination therapy compared to monotherapy.

Immunohistochemical Analysis of Tumor Tissue

We observed the pathological section of the tumor tissue after treatment (Figure S3). As can be seen from the 4 groups of images, the combination treatment of LNP/siMETTL16 and LNP/MUC1 (G4) significantly reduced the severity of TNBC. And at the same time, we also performed immunohistochemical analysis on METTL16, N-cadherin and E-cadherin in tumor tissues, which are closely related to tumor invasion. As shown in Figure 3A, the distribution and intensity of the brown area in the field of view of G2 and G4 were significantly smaller than those in PBS group, which

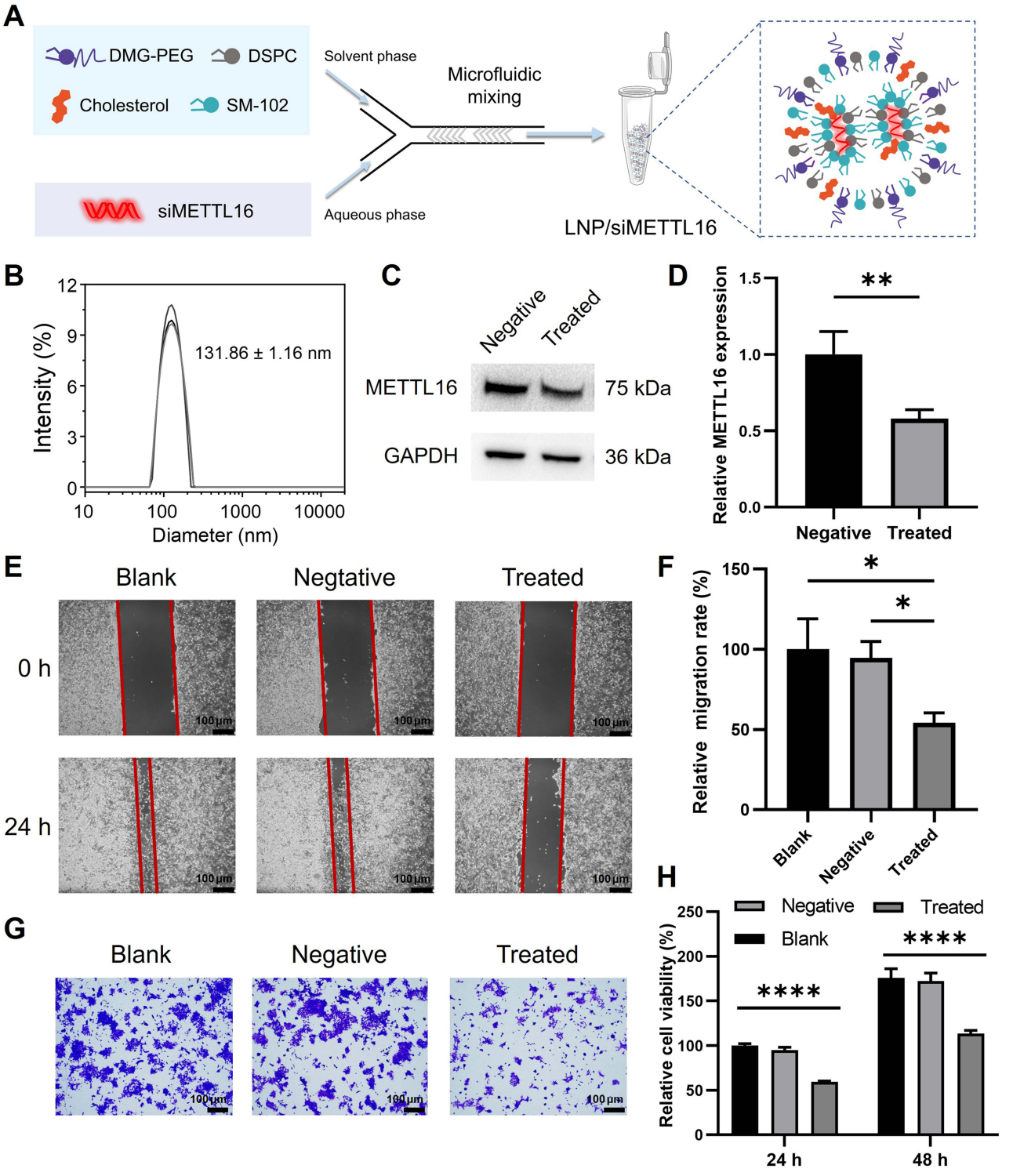

Figure 1 Preparation, characterization, and in vitro antitumor activity of LNP/siMETTL16. Blank, Negative and Treated represent PBS, empty LNP and LNP/siMETTL16, respectively. (**A**) Preparation of LNP/siMETTL16 using microfluidic technology. (**B**) Particle size distribution of LNP/siMETTL16. (**C** and **D**) METTL16 expression in 4T1 cells after 24h transfection with LNP/siMETTL16. (**E** and **F**) Cell migration after 24h of incubation of LNP/siMETTL16 with 4T1 cells. (**G**) Crystal Violet Staining Images of 4T1 cells incubated with LNP/siMETTL16 for 24h. (**H**) Cell viability using the CCK-8 assay for 4T1 cells incubated with LNP/siMETTL16. Data were presented as the mean ± SD (*p < 0.05, **p < 0.01, ****p < 0.0001).

https://doi.org/10.2147/IJN.S520329

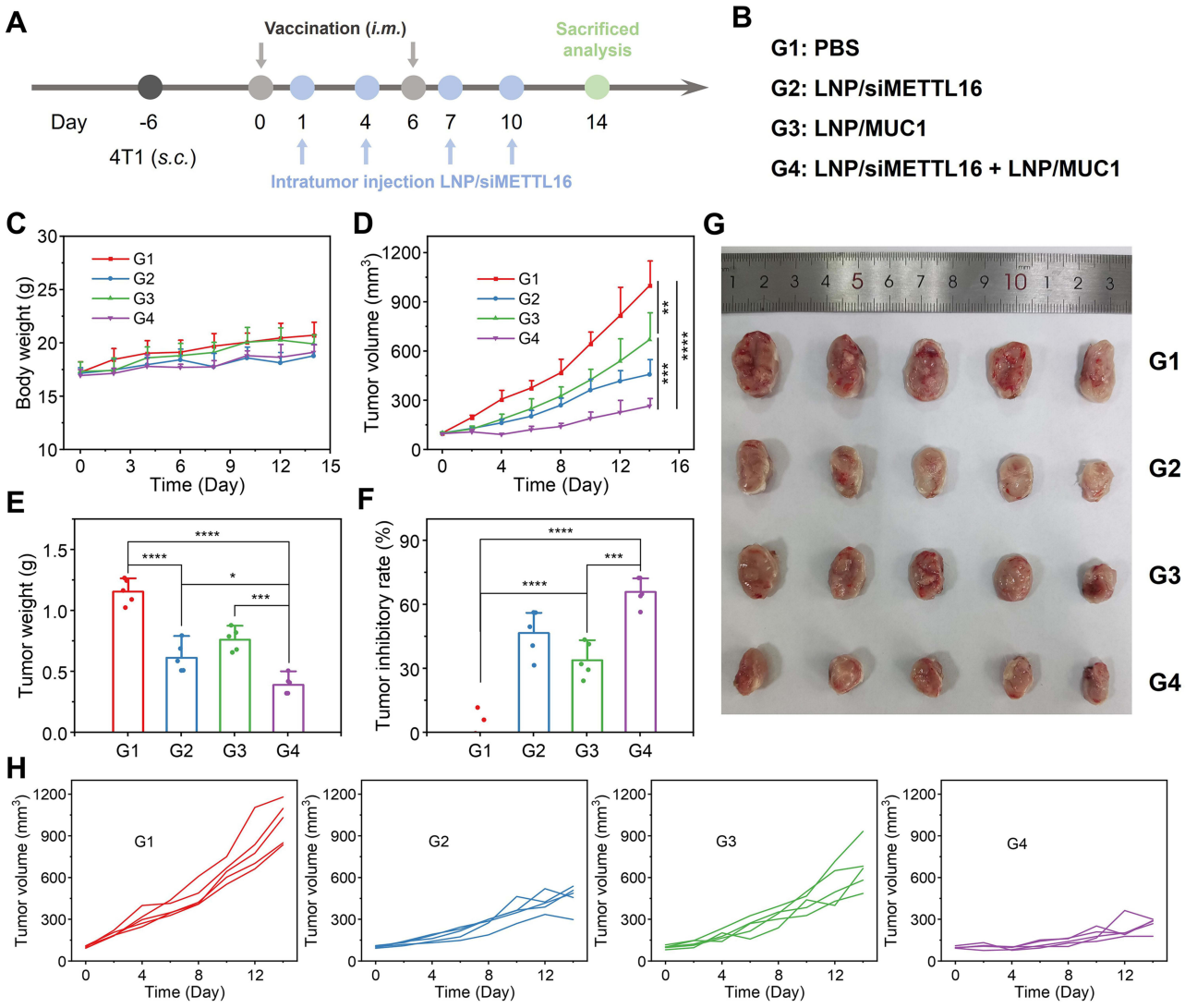

Figure 2 LNP/siMETTL16 and LNP/mMUC1 vaccine combined therapy for TNBC. (**A**) Establishment of 4T1 subcutaneous tumor model and treatment plan. (**B**) Different treatment groups. (**C**) Body weight change curves of mice. (**D**) Tumor volume growth curves. (**E**) Average tumor mass. (**F**) Tumor inhibition rates based on mass. (**G**) Anatomical images of tumors after treatment. (**H**) Tumor volume growth curves for individual mice in each group. Data were presented as the mean ± SD (*p < 0.05, **p < 0.01, ***p < 0.001, ****p < 0.0001).

proved that LNP/siMETTL16 successfully inhibited the expression of METTL16 protein in vivo. In addition, careful observation revealed that cadherin, known as the "switch" for tumor invasion, also reversed in the combined treatment group, that was, N-cadherin was downregulated and E-cadherin was upregulated compared with G1 (Figure 3B and C). The above results demonstrate that LNP/siMETTL16 successfully inhibited tumor invasion and migration through gene regulation, providing valuable therapeutic time to support the slow immune activation process of tumor vaccines.

Immune Status Analysis of Tumor and Lymphoid Tissues

The tumor suppression effect mediated by both mRNA vaccines and gene silencing is inseparable from the body's immune status. Therefore, we dissected the spleen and tumor tissues for flow cytometry analysis after treatment. Figure 4A and B show the proportion of $CD8^+$ T cells and central memory T cells (T_{CM}) in the spleen, which was significantly higher in G3 than in G1, and this was attributed to the mRNA tumor vaccine promoting the proliferation of $CD8^+$ T and T_{CM} cells. The combined treatment group (G4) showed the highest ratio, indicating that silencing of METTL16 has a certain promoting effect on the body's immune

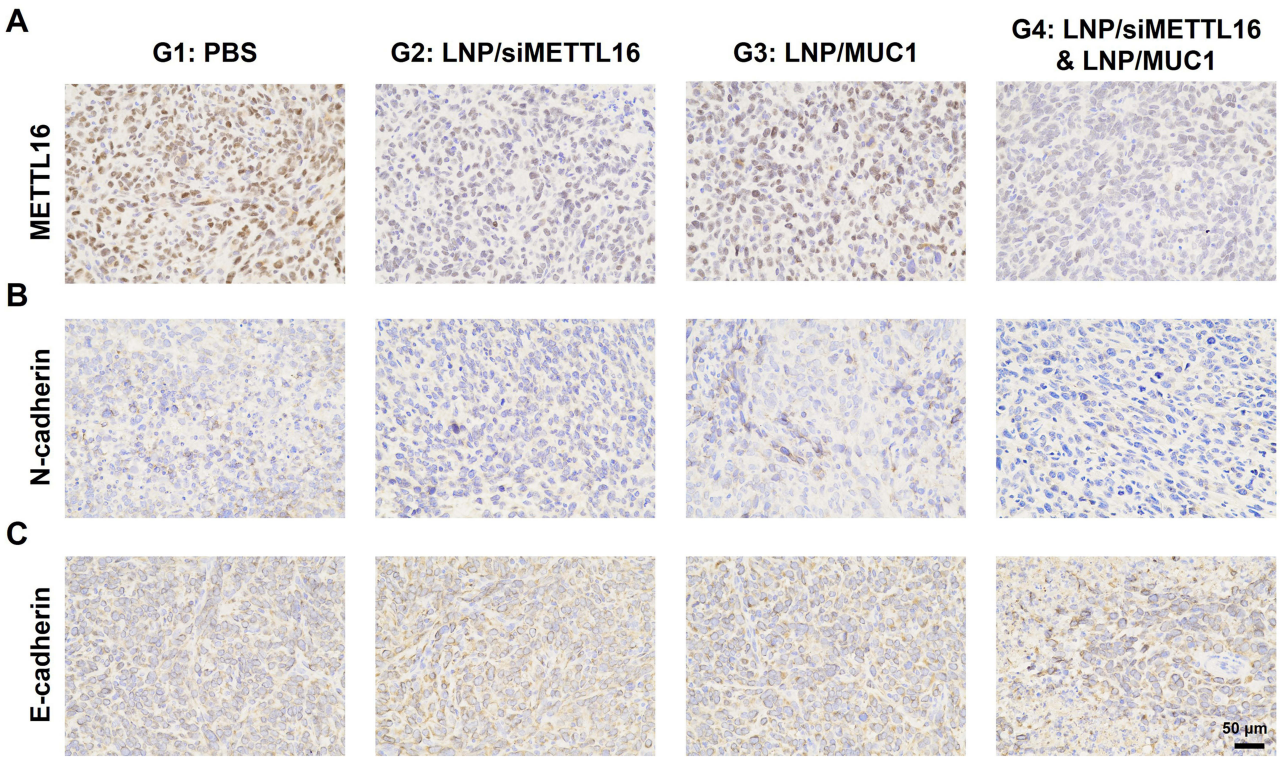

Figure 3 Immunohistochemical analysis of tumor tissues after different treatment methods. (**A**) METTL16 (**B**) N-cadherin and (**C**) E-cadherin. Scale bar = 50 μm.

activation. This phenomenon may be related to inhibiting the methylation of METTL16 which was decreasing the expression of FBXO5 and promoting ER stress-induced cell apoptosis, thereby preventing the progression of tumor cell.[38]

In addition, the evaluation results of immune cells in the tumor microenvironment were even more striking. As shown in Figure 4C, G4 exhibited the highest proportion of mature dendritic cells (DCs), outperforming both G2 and G3. This finding suggested that the apoptosis induced by targeting METTL16 may facilitate the maturation of local DCs and subsequent activation of T lymphocytes. Exhilaratingly, $CD3^+$ T cells and $CD3^+$ $CD8^+$ T cells demonstrated a consistent trend, indicating an elevated infiltration ratio of T lymphocytes within tumor tissues following combined therapy, which was conducive to tumor suppression (Figure 4D–G). The observed phenomena were hypothesized to be attributable to the mitigation of lesion malignancy by LNP/siMETTL16, thereby promoting the maturation and infiltration of immune cells. It is well-established that tumor-associated macrophages (TAMs) play a pivotal role in regulating the tumor immune microenvironment, with M1 macrophages, in particular, often exerting anti-tumor effects by secreting pro-inflammatory cytokines, directly inducing tumor cell lysis, and presenting antigens to T cells.[39] Consequently, we also investigated the proportion of M1 macrophages in tumors, which showed a similar trend, further confirming the validity of the above hypothesis (Figure 4F).

SORT-LNP/siMETTL16 Targets the Lung

It has been reported that the lung is one of the common metastatic sites for triple-negative breast cancer, and patients with lung metastasis often have poor prognosis and relatively short survival.[40] Therefore, developing formulations targeting METTL16 as a therapeutic target for breast cancer lung metastasis are highly necessary.

Liver accumulation is an important obstacle in developing therapeutically effective nanoparticle delivery systems.[41] Previous studies have shown that Selective ORgan Targeting (SORT) nanoparticles can effectively solve this problem. SORT added to conventional lipid vectors leaded to the generation of different surface chemical compositions beneath the PEG layer. Through protein adsorption, it altered the surface composition of SORT LNPs, thereby generating unique nanodomains. Researchers have found that 1,2-dioleoyl-3-trimethylammonium-propane (DOTAP) which is a quaternary

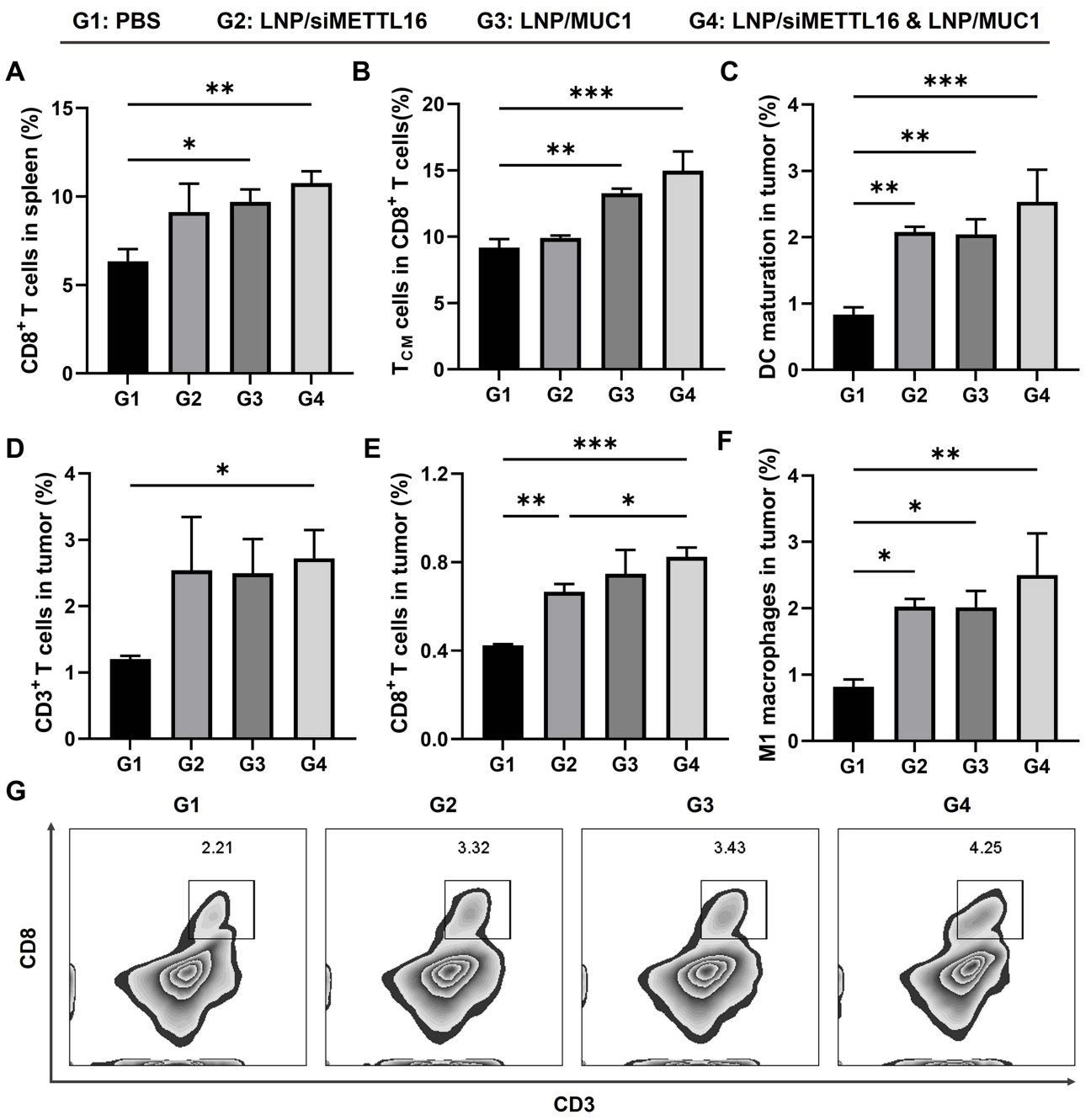

Figure 4 Assessment of immune status after treatment. (**A**) Quantitative analysis of $CD8^+$ T cells in the spleen. (**B**) Quantitative analysis of T_{CM} ($CD62L^+$ $CD44^+$) cells among spleen $CD8^+$ T cells. (**C**–**F**) Quantitative analysis of (**C**) $CD45^+$ $CD11c^+$ $CD80^+$ mature DCs, (**D**) $CD45^+$ $CD3^+$ T cells, (**E**) $CD45^+$ $CD3^+$ $CD8^+$ T cells and (**F**) M1 macrophages ($CD45^+$ $F4/80^+$ $CD80^+$) in the tumor. (**G**) Representative flow cytometry plots of $CD45^+$ $CD3^+$ $CD8^+$ T cells in tumor tissues. Data were presented as the mean ± SD (*p < 0.05, **p < 0.01, ***p < 0.001).

amino lipid (a permanently cationic lipid) can enhance lung targeting.[42] To improve the efficacy of the nanoformulation, according to the synthesis method of lung targeting vector, we introduced the positively charged lipid molecule DOTAP into LNP components,[43] successfully preparing SORT-LNP for the pulmonary targeted delivery of nucleic acid drugs (Figure S1), and the hydrodynamic diameter (Figure S2B), PDI and encapsulation rate were measured (Table S3).

First, we performed live imaging of mice injected with LNP/Luc-mRNA/DIR and SORT- LNP/Luc-mRNA//DIR after 6h. Figure 5A shows that there was a strong fluorescence signal of DIR in the liver, and no obvious trend of lung metastasis was observed. Then, we performed live imaging on mice to observe whether there was obvious lung targeting

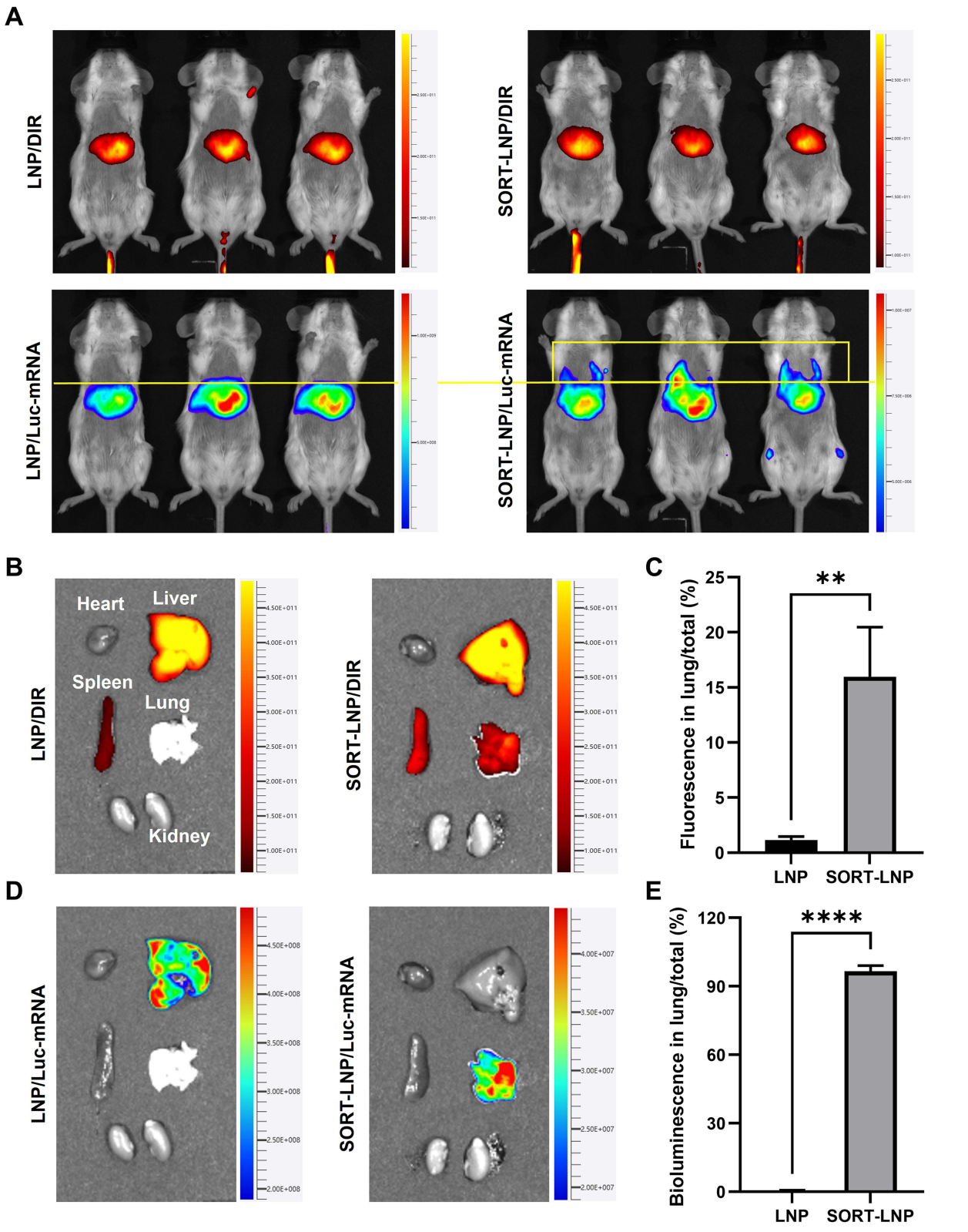

Figure 5 Six hour after intravenous injection of LNP and SORT-LNP in vivo imaging analysis. (**A**) Live images of mice with DIR probe fluorescence and fluorescent pigmented enzyme bioluminescence (Luc-mRNA) images. (**B**) DIR probe fluorescence imaging of various organs. (**C**) Comparative analysis of DIR fluorescence intensity in lung tissue. (**D**) Fluorescent pigmented enzyme bioluminescence (Luc-mRNA) imaging of various organs. (**E**) Comparative analysis of bioluminescence intensity in lung tissue. Images were analyzed using Living Image software (PerkinElmer). Biological replicates of the experiment (n = 3). Data were presented as the mean ± SD (**p < 0.01, ****p < 0.0001).

https://doi.org/10.2147/IJN.S520329

fluorescence. As shown in Figure 5A, under the same horizontal line (yellow line), we could observe that there was lung fluorescence (circled by the yellow box) in SORT-LNP group, but it was not obvious. Considering that the lung and liver were too close in vivo, which affected the observation. Because the liver and lung fluorescence zoning were not obvious, fluorescence quantitative analysis cannot be performed; next, we separated the organs and performed in vivo organ imaging to verify above conjecture. As shown in Figure 5B, SORT-LNP successfully accumulated in the lungs 6 hours after intravenous administration, as shown in Figure 5C, SORT-LNP with DIR increasing the pulmonary accumulation rate of the classic LNP from 1.2% to 16%. As a result of Figure S4A, SORT-LNP with DIR demonstrated more than 90% of fluorescent signal. However, upon closer inspection, no significant change in fluorescence intensity was observed in the liver; this was consistent with the luminescent characteristics of DIR labeled LNPS delivered in vivo. Since the liver and spleen are two main organs where most LNPs accumulate after systemic delivery.[44–46] Thus, we believed that when using DIR fluorescent dye, the lipid nanoparticles targeting the carrier not only show fluorescence in the targeted organs, but also accumulated in the liver as it circulates after systemic delivery due to the leakage of DIR dye caused by the rupture of the lipid molecular layer, resulting in both DIR fluorescence in the targeted organs and liver. At the same time, we also validated the correctness of the above hypothesis by delivering a luciferase reporter gene (Luc-mRNA). As shown in Figure 5D, LNP produced bright bioluminescence primarily in the liver, while SORT-LNP predominantly localized to the lungs up to 96.5% (Figure 5E). Quantification of fluorescence showed that more than 85% of the signal was produced from SORT-LNP (Figure S4B), indicating that it successfully delivered the nucleic acid to the lungs and enabled expression. In order to make the experimental results more convincing, the organ fluorescence images of the three groups of mice were shown in Figure S4C and D. Therefore, the introduction of SORT-LNP provides favorable support for the delivery of siMETTL16 to lung lesion tissues and realizes the gene regulation.

SORT-LNP/siMETTL16 and LNP/mMUC1 Combination Therapy for TNBC Lung Metastases

After successfully validating the effective lung-targeted delivery of SORT-LNP, we further explored the combined inhibitory effect of SORT-LNP/siMETTL16 and LNP/mMUC1 on lung metastasis of TNBC. The treatment protocol is illustrated in Figure 6A. First, a lung metastasis model was established by injecting a suspension of 4T1 cells into mice via the tail vein. Treatment commenced 6 days later, with SORT-LNP/siMETTL16 administered via intravenous injection and LNP/mMUC1 via intramuscular injection. On the tenth day, the mice were euthanized, and their organs were dissected and analyzed.

Figure 6B shows the lung tissues after treatment. In the PBS group (G1), the lung surface was extensively covered with nodules, whereas the single-treatment groups (G3, G4) exhibited a noticeable reduction. Excitingly, in the combined treatment group (G5), large nodules were nearly absent, demonstrating the superior tumor-suppressing efficacy of the combination therapy. Strikingly, the therapeutic effect of lung-targeted delivery in G3 was significantly better than that in G2, further underscoring the necessity of incorporating SORT-LNP.

Moreover, we observed the internal lung tissue morphology through H&E staining (Figure 6C). In G1, the internal tissue was almost entirely occupied by tumors, while G5 predominantly displayed a normal structure. Lung mass showed a similar trend, with the mass in G1 (laden with nodules) being 3.57 times higher than that in G5 (Figure 6D). The above results demonstrate that our therapeutic strategy effectively mitigates lungs metastasis of tumors and holds promising potential for clinical application.

Biosafety Analysis

In the above study, we primarily focused on the antitumor efficacy of LNP/siMETTL16. However, its biosafety was equally important and cannot be overlooked. In addition to monitoring the body weight of mice during the treatment process (Figure 2C), H&E staining analysis of the major organs of mice was performed after treatment. As shown in Figure S5, no significant organ toxicity or tissue necrosis was observed in the heart, liver, spleen, lungs, or kidneys across the treatment groups. This was closely associated with the advantages of LNP, including efficient delivery, biodegradability, and low toxicity.

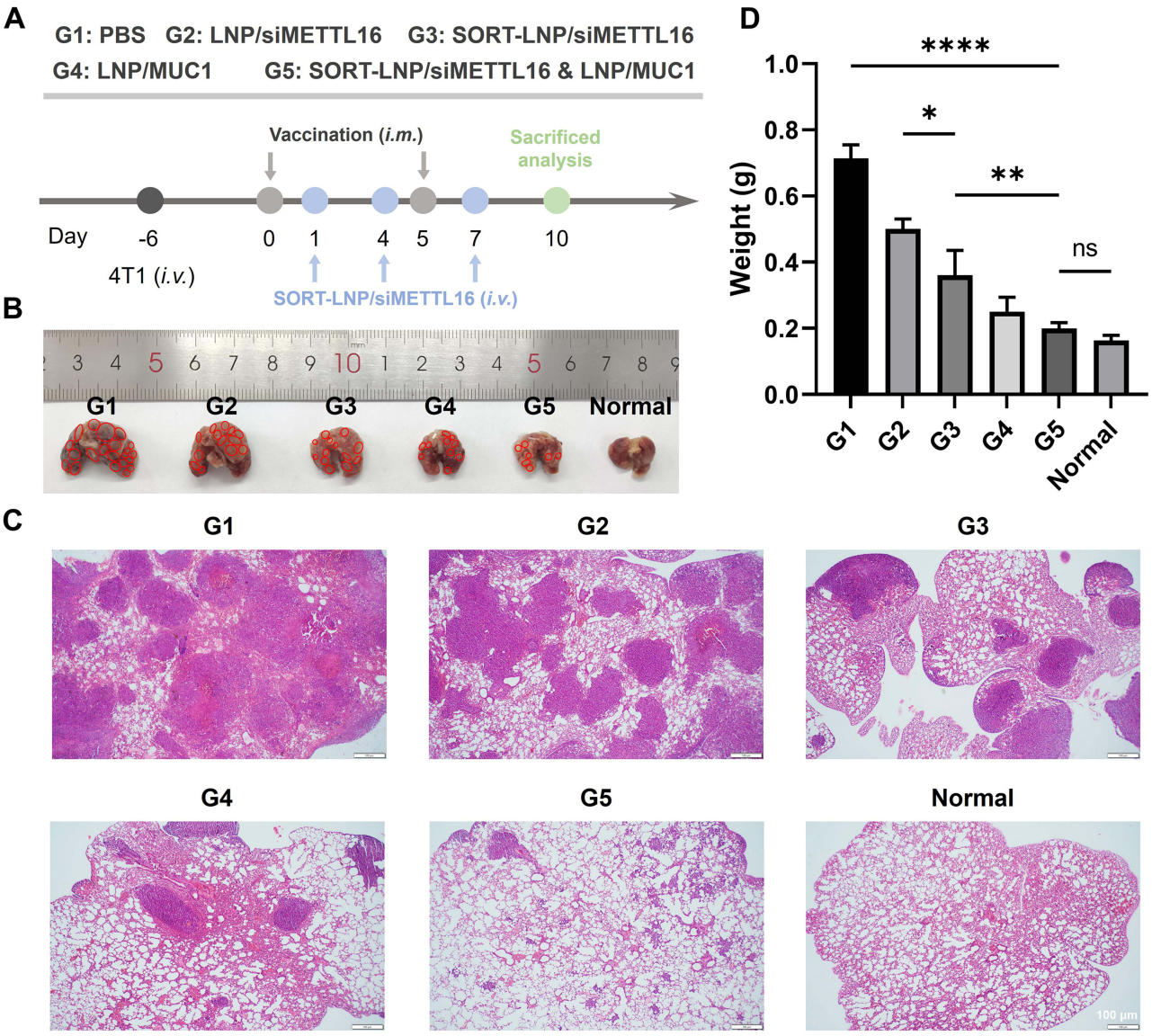

Figure 6 Combined therapy of SORT-LNP/siMETTL16 and LNP/mMUC1 for TNBC lung metastasis. (**A**) Establishment of 4T1 lung metastasis model and treatment protocol. (**B**) Tumor volume changes and analysis of lung metastatic nodules after treatment. Metastatic nodules were indicated with red circles in bright field images. (**C**) H&E-stained results of lung tissues after treatment. (**D**) Comparative analysis of lung organ mass after treatment. Data were presented as the mean ± SD (*$p < 0.05$, **$p < 0.01$ ****$p < 0.0001$).

Discussion

As an emerging immunotherapy in recent years, mRNA vaccines are unique in that they can encode specific antigen proteins, thereby stimulating the body to produce a strong immune response. In this study, we successfully expressed the protein of specific antigen by using the mRNA vaccine of MUC1. As shown in Figure 1–3, LNP/siMETTL16 had obvious tumor suppressive effect in vivo and in vitro, and can improve the tumor microenvironment (Figure 4), which has shown that it can promote the formation of immune microenvironment, that laid the foundation for precision treatment. Moreover, we innovatively constructed SORT-LNP/siMETTL16 targeting the lung by introducing the lung targeting vector (SORT), successfully introduced the target gene silencing into the lung, and successfully inhibited the lung metastasis of TNBC. However, according to the combined treatment results of this study, Figure 3A shows that the treatment of LNP/MUC1 also seemed to be able to inhibit the expression of METTL16. How to determine and explain the mechanism of action of LNP/MUC1 and METTL16 was currently under in-depth study. Our preliminary data obtained shown that the two complement each other in the tumor immune microenvironment. The results of these investigations will be published in future manuscripts.

https://doi.org/10.2147/IJN.S520329

Although our work provided a new target (METTL6) and strategy for clinical treatment of TNBC, however, this study also had certain limitations. For example, there were still differences between the experimental model and the real human environment, so it was particularly important to better simulate the in vivo conditions to explore the experimental conditions. In addition, the long-term effectiveness and drug resistance of combination therapy as well as prognosis survival tracking also needed to be further evaluated.

Conclusion

In this study, we successfully developed a nanoformulation targeting METTL16 target in TNBC and its tumor suppressive effect and the enhancing effect of mRNA vaccine were verified in the 4T1 tumor-bearing mouse model. Furthermore, we also constructed lung-targeted SORT-LNP/siMETTL16 formulation by utilizing organ-selective lung targeting vectors to combat TNBC lung metastases. In combination with mRNA tumor vaccines, the nanoformulation similarly and efficiently mitigated TNBC lung metastasis. This ideal tumor-suppressing effect arises from three primary sources: firstly, direct inhibition of tumor invasion and migration through knock-down of the METTL16 target; secondly, as the malignancy of tumor foci diminishes, the activation and infiltration of immune cells within tumor microenvironment also undergo enhancement, directly facilitating the antitumor effects mediated by the vaccine; thirdly, the rapid action of siMETTL16, which buys valuable treatment time for the slow immune activation process of the vaccine. Consequently, our work provides substantial support for the clinical utility of the METTL16 target and introduces a novel strategy for combination therapy of mRNA tumor vaccines.

Abbreviations

TNBC, Triple-negative breast cancer; LNP, lipid nanoparticle; SORT, Selective ORgan-Targeting; METTL16, a methyltransferase-like protein; i.v., intravenous injection.

Data Sharing Statement

These data of this paper can be available from the corresponding authors on reasonable request.

Author Contributions

All authors made a significant contribution to the work reported, whether in the conception, study design, execution, acquisition of data, analysis, and interpretation, or in all these areas, took part in drafting, revising, or critically reviewing the article; gave final approval of the version to be published; have agreed on the journal to which the article has been submitted; and agree to be accountable for all aspects of the work.

Funding

This work was financially supported by Liaoning Provincial Science and Technology Program Joint Fund (2023JH2/101700343), Dalian Key Research and Development Program (2030YF20SN038), the Fundamental Research Funds for the Central Universities (DUT24YG120), the Interdisciplinary Innovation Project of the Second Affiliated Hospital of Dalian Medical University (2022JCXKYB20 and 2022JCXKYB01).

Disclosure

Yufeng Zhang reports grants from Department of Science & Technology of Liaoning province, Dalian Municipal Science and Technology Bureau, the Second Affiliated Hospital of Dalian Medical University and Ministry of Education of the People's Republic of China, during the conduct of the study. The other authors report no conflicts of interest in this work.

References

1. Arnold M, Morgan E, Rumgay H, et al. Current and future burden of breast cancer: global statistics for 2020 and 2040. *Breast*. 2022;66:15–23. doi:10.1016/j.breast.2022.08.010
2. Jain A, Barge A, Parris CN. Combination strategies with PARP inhibitors in BRCA-mutated triple-negative breast cancer: overcoming resistance mechanisms. *Oncogene*. 2024;44:193–207. doi:10.1038/s41388-024-03227-6
3. Niu Z, Wu J, Zhao Q, et al. CAR-based immunotherapy for breast cancer: peculiarities, ongoing investigations, and future strategies. *Front Immunol*. 2024;15:1385571. doi:10.3389/fimmu.2024.1385571

4. Wu S, Zheng Y, Olopade OI. The convergence of genomic medicine and translational omics in transforming breast cancer patient care. *J Clin Invest*. 2024;134(21):e187520. doi:10.1172/JCI187520
5. Tong Y, Fan X, Liu H, et al. Advances in Trop-2 targeted antibody-drug conjugates for breast cancer: mechanisms, clinical applications, and future directions. *Front Immunol*. 2024;15:1495675. doi:10.3389/fimmu.2024.1495675
6. Qu Y, Xu J, Zhang T, et al. Advanced nano-based strategies for mRNA tumor vaccine. *Acta Pharm Sin B*. 2024;14(1):170–189. doi:10.1016/j.apsb.2023.07.025
7. Yuan Y, Gao F, Chang Y, et al. Advances of mRNA vaccine in tumor: a maze of opportunities and challenges. *Biomark Res*. 2023;11(1):6. doi:10.1186/s40364-023-00449-w
8. Esprit A, Mey W, Bahadur SR, et al. Neo-antigen mRNA vaccines. *Vaccines*. 2020;8(4):776. doi:10.3390/vaccines8040776
9. Jiang XT, Liu Q. mRNA vaccination in breast cancer: current progress and future direction. *J Cancer Res Clin Oncol*. 2023;149(11):9435–9450. doi:10.1007/s00432-023-04805-z
10. Sayour EJ, Boczkowski D, Mitchell DA, et al. Cancer mRNA vaccines: clinical advances and future opportunities. *Nat Rev Clin Oncol*. 2024;21(7):489–500. doi:10.1038/s41571-024-00902-1
11. Rojas LA, Sethna Z, Soares KC, et al. Personalized RNA neoantigen vaccines stimulate T cells in pancreatic cancer. *Nature*. 2023;618(7963):144–150. doi:10.1038/s41586-023-06063-y
12. Weber J, Poh A. mRNA vaccine slows melanoma recurrence. *Cancer Discov*. 2023;13(6):1278.
13. Lan Y, Ni W, Tai G. Expression of MUC1 in different tumours and its clinical significance (Review). *Mol Clin Oncol*. 2022;17(6):161. doi:10.3892/mco.2022.2594
14. Apostolopoulos V, Pietersz GA, Tsibanis A, et al. Pilot Phase III immunotherapy study in early-stage breast cancer patients using oxidized mannan-MUC1 [ISRCTN71711835]. *Breast Cancer Res*. 2006;8(3):R27. doi:10.1186/bcr1505
15. Nath S, Mukherjee P. MUC1: a multifaceted oncoprotein with a key role in cancer progression. *Trends Mol Med*. 2014;20(6):332–342. doi:10.1016/j.molmed.2014.02.007
16. Musicus AA, Roberto CA, Moran AJ, et al. Effect of front-of-package information, fruit imagery, and high-added sugar warning labels on parent beverage choices for children: a randomized clinical trial. *JAMA Network Open*. 2022;5(10):e2236384. doi:10.1001/jamanetworkopen.2022.36384
17. Park WY, Shin N, Kim JY, et al. Pathologic definition and number of lymphovascular emboli: impact on lymph node metastasis in endoscopically resected early gastric cancer. *Hum Pathol*. 2013;44(10):2132–2138. doi:10.1016/j.humpath.2013.04.006
18. Mukherjee P, Ginardi AR, Madsen CS, et al. MUC1-specific CTLs are non-functional within a pancreatic tumor microenvironment. *Glycoconjugate J*. 2001;18(11–12):931–942. doi:10.1023/A:1022260711583
19. Mukherjee P, Tinder TL, Basu GD, Pathangey LB, Chen L, Gendler SJ. Therapeutic efficacy of MUC1-specific cytotoxic T lymphocytes and CD137 co-stimulation in a spontaneous breast cancer model. *Breast Dis*. 2004;20:53–63. doi:10.3233/BD-2004-20107
20. Jiang Z, Xu Y, Du G, Sun X. Emerging advances in delivery systems for mRNA cancer vaccines. J. *Control Release*. 2024;370:287–301. doi:10.1016/j.jconrel.2024.04.039
21. Salewski I, Kuntoff S, Kuemmel A, et al. Combined vaccine-immune-checkpoint inhibition constitutes a promising strategy for treatment of dMMR tumors. *Cancer Immunol Immunother*. 2021;70(12):3405–3419. doi:10.1007/s00262-021-02933-4
22. Fu R, Qi R, Xiong H, et al. Combination therapy with oncolytic virus and T cells or mRNA vaccine amplifies antitumor effects. *Signal Transduct Target Ther*. 2024;9(1):118. doi:10.1038/s41392-024-01824-1
23. Yang A, Bai Y, Dong X, et al. Hydrogel/nanoadjuvant-mediated combined cell vaccines for cancer immunotherapy. *Acta Biomater*. 2021;133:257–267. doi:10.1016/j.actbio.2021.08.014
24. Soltani M, Savvateeva LV, Ganjalikhani-Hakemi M, Zamyatnin AA. Clinical combinatorial treatments based on cancer vaccines: combination with checkpoint inhibitors and beyond. *Curr Drug Targets*. 2022;23(11):1072–1084. doi:10.2174/1389450123666220421124542
25. Rodrigues MC, Morais JAV, Ganassin R, et al. An overview on immunogenic cell death in cancer biology and therapy. *Pharmaceutics*. 2022;14(8):1564. doi:10.3390/pharmaceutics14081564
26. Mendes BB, Conniot J, Avital A, et al. Nanodelivery of nucleic acids. *Nat Rev Meth Primers*. 2022;2:24. doi:10.1038/s43586-022-00104-y
27. Jia Y, Wang X, Li L, et al. Lipid nanoparticles optimized for targeting and release of nucleic acid. *Adv Mater*. 2024;36(4):2305300. doi:10.1002/adma.202305300
28. Liu L, Wang Y, Miao L, et al. Combination immunotherapy of MUC1 mRNA nano-vaccine and CTLA–4 blockade effectively inhibits growth of triple negative breast cancer. *Mol Ther*. 2018;26(1):45–55. doi:10.1016/j.ymthe.2017.10.020
29. Kulkarni JA, Cullis PR, van der Meel R. Lipid nanoparticles enabling gene therapies: from concepts to clinical utility. *Nucleic Acid Ther*. 2018;28(3):146–157. doi:10.1089/nat.2018.0721
30. Cheng Q, Wei T, Farbiak L, Johnson LT, Dilliard SA, Siegwart DJ. Selective organ targeting (SORT) nanoparticles for tissue-specific mRNA delivery and CRISPR-Cas gene editing. *Nat Nanotechnol*. 2020;15(4):313–320. doi:10.1038/s41565-020-0669-6
31. Ma R, Li Y, Su Y, et al. Lipid nanoparticles: a delicate nucleic acid delivery system to be further explored. *Nano Today*. 2025;61:102586. doi:10.1016/j.nantod.2024.102586
32. Xu M, Qi Y, Liu G, et al. Size-dependent in vivo transport of nanoparticles: implications for delivery, targeting, and clearance. *ACS Nano*. 2023;17(21):20825–20849. doi:10.1021/acsnano.3c05853
33. Swanton C, Bernard E, Abbosh C, et al. Embracing cancer complexity: hallmarks of systemic disease. *Cell*. 2024;187(7):1589–1616. doi:10.1016/j.cell.2024.02.009
34. Liu S, Zhang X, Wang W, et al. Metabolic reprogramming and therapeutic resistance in primary and metastatic breast cancer. *Mol Cancer*. 2024;23(1):261. doi:10.1186/s12943-024-02165-x
35. Ji J, Jing A, Ding Y, et al. FBXO5-mediated RNF183 degradation prevents endoplasmic reticulum stress-induced apoptosis and promotes colon cancer progression. *Cell Death Dis*. 2024;15(1):33. doi:10.1038/s41419-024-06421-2
36. Wu Z, Zhou J, Chen F, et al. 13-Methyl-palmatrubine shows an anti-tumor role in non-small cell lung cancer via shifting M2 to M1 polarization of tumor macrophages. *Int Immunopharmacol*. 2022;104:108468. doi:10.1016/j.intimp.2021.108468
37. Yu P, Han Y, Meng L, et al. The incorporation of acetylated LAP-TGF-β1 proteins into exosomes promotes TNBC cell dissemination in lung micrometastasis. *Mol Cancer*. 2024;23(1):82. doi:10.1186/s12943-024-01995-z

38. Tang Y, Li C. Recent progress in the strategies to construct long-circulating nano-drug delivery system and related researches. *Prog Pharmaceut Sci*. 2018;42(11):816–823.
39. Dilliard SA, Cheng Q, Siegwart DJ. On the mechanism of tissue-specific mRNA delivery by selective organ targeting nanoparticles. *Proc Natl Acad Sci U S A*. 2021;118(52):e2109256118. doi:10.1073/pnas.2109256118
40. Wang X, Liu S, Sun Y, et al. Preparation of selective organ-targeting (SORT) lipid nanoparticles (LNPs) using multiple technical methods for tissue-specific mRNA delivery. *Nat Protoc*. 2023;18(1):265–291. doi:10.1038/s41596-022-00755-x
41. Luozhong S, Yuan Z, Sarmiento T, et al. Phosphatidylserine lipid nanoparticles promote systemic RNA delivery to secondary lymphoid organs. *Nano Lett*. 2022;22(20):8304–8311. doi:10.1021/acs.nanolett.2c03234
42. Fenton OS, Kauffman KJ, Kaczmarek JC, et al. Synthesis and biological evaluation of ionizable lipid materials for the in vivo delivery of messenger RNA to B lymphocytes. *Adv Mater*. 2017;29(33). doi:10.1002/adma.201606944
43. Shi B, Keough E, Matter A, et al. Biodistribution of small interfering RNA at the organ and cellular levels after lipid nanoparticle-mediated delivery. *J Histochem Cytochem*. 2011;59(8):727–740. doi:10.1369/0022155411410885
44. Qi R, Fu R, Xiong H, et al. Combination therapy with oncolytic virus and T cells or mRNA vaccine amplifies antitumor effects. *Signal Transduct Target Ther*. 2024;9(6):2655–2668.
45. Mandula JK, Chang S, Mohamed E, et al. Ablation of the endoplasmic reticulum stress kinase PERK induces paraptosis and type I interferon to promote anti-tumor T cell responses. *Cancer Cell*. 2022;40(10):1145–1160.e9. doi:10.1016/j.ccell.2022.08.016
46. Wang R, Gao X, Xie L, et al. METTL16 regulates the mRNA stability of FBXO5 via m6A modification to facilitate the malignant behavior of breast cancer. *Cancer Metab*. 2024;12(1):22. doi:10.1186/s40170-024-00351-5